Development of an antenna and multipath calibration system for Global Positioning System sites

K.-D. Park,[1,2] P. Elósegui,[1,3] J. L. Davis,[1] P. O. J. Jarlemark,[1,4] B. E. Corey,[5] A. E. Niell,[5] J. E. Normandeau,[1,6] C. E. Meertens,[7] and V. A. Andreatta[7]

[1] Site-dependent errors such as antenna phase-center variations, multipath, and scattering can have a significant effect on high-precision applications of the Global Positioning System (GPS). Determination of these errors has proven to be elusive since no method has been developed to measure these effects accurately in situ. We have designed and constructed a prototype Antenna and Multipath Calibration System (AMCS) to obtain such in situ corrections. The primary components of the AMCS are a steerable parabolic antenna, two GPS receivers, and a computer for control and data-logging functions. We obtain phase corrections for site-dependent errors by forming the difference between the carrier-beat phases from the GPS antenna to be calibrated and from the AMCS antenna, which is relatively free of such errors. Preliminary "sky maps" of the antenna phase and multipath contributions show root-mean-square (RMS) phase variations that are a factor of 10 or more greater than the AMCS system noise, which is ~0.5 mm. To explore the source of this "noise," we acquired observations over small (few degrees) patches of the sky. From the analysis of these experiments we concluded that the source of the phase variations was antenna and multipath errors that vary by ~5 mm amplitude over small changes in satellite direction. Thus, for example, differences of 1° in elevation angle can result in several millimeter variations in phase. Similarly, small variations in azimuth angle can also result in significant phase variations. We have also observed day-to-day millimeter-level changes in the calibration. We hypothesize that these phase variations are due to changes in multipath caused by changes in the local electromagnetic environment associated with, e.g., weather. *INDEX TERMS:* 0609 Electromagnetics: Antennas; 1243 Geodesy and Gravity: Space geodetic surveys; 1247 Geodesy and Gravity: Terrestrial reference systems; 1294 Geodesy and Gravity: Instruments and techniques; 6994 Radio Science: Instruments and techniques; *KEYWORDS:* GPS multipath calibration, antennas, geodesy

1. Introduction

[2] Two important sources of error for precise geodesy with the Global Positioning System (GPS) are phase multipath and scattering [e.g., *Elósegui et al.*, 1995; *Axelrad et al.*, 1996; *Byun et al.*, 2002] and direction-dependent variations in the antenna phase center [e.g., *Rothacher et al.*, 1995; *Mader and MacKay*, 1996; *Wübbena et al.*, 2000]. These site-dependent problems have the potential to adversely affect geodetic applica-

---

[1]Harvard-Smithsonian Center for Astrophysics, Cambridge, Massachusetts, USA.

[2]Now at GPS Research Group, Korea Astronomy Observatory, Daejeon, and College of Forest Science, Kookmin University, Seoul, Korea.

[3]Also at Institut d'Estudis Espacials de Catalunya/CSIC, Barcelona, Spain.

[4]Now at Swedish National Testing and Research Institute, Borås, Sweden.

[5]MIT Haystack Observatory, Westford, Massachusetts, USA.

[6]Now at UNAVCO, Inc., Boulder, Colorado, USA.

[7]UNAVCO, Inc., Boulder, Colorado, USA.

tions that utilize the carrier-beat phase observable [e.g., *Leick*, 1995]. The problems stem from the basic design of GPS antennas, which are required to accept radiation from multiple directions simultaneously. These errors affect all parameters that are estimated from the GPS phase data, including site position (and hence velocity) and the neutral atmospheric propagation delays. For example, *Schmid and Rothacher* [2003] created a self-consistent set of GPS receiver and satellite antenna phase patterns and phase center offsets and showed that a change to this set has an influence on estimates of site position and troposphere parameters. Furthermore, although no detailed studies have ever been performed, it is logical to assume that errors in the estimated satellite orbital positions due to multipath, scattering, and phase-center variations are commensurate with those of other parameters.

[3] Geodetic GPS has most recently been moving from traditional 30 s data collection periods suitable for global tectonic motion studies to periods of 1 s or less for a variety of geophysical applications, such as seismology [e.g., *Larson et al.*, 2003] and volcanology. Because these emerging applications require instantaneous positioning at high rates, the old (and wishful) assumption that site-dependent errors would average out is no longer correct, and thus they need to be properly considered.

[4] A number of studies have been conducted to address site-dependent errors. The earliest modeling studies [e.g., *Georgiadou and Kleusberg*, 1988] were based on reflection from a simple horizontal ground surface. *Elósegui et al.* [1995] found that these simple models worked fairly well for near-field signal scattering as well. (Near-field scattering is the term used when electrical currents excited in the reflectors must be taken into account.) Such simple models cannot, however, capture the unique and complex geometry at each GPS site, though they seem to be useful for the largest multipath errors. *Axelrad et al.* [1996] developed a method for inferring multipath from recorded signal-to-noise ratio (SNR) variations. This approach, though it appears promising, might ultimately be limited by the accuracy of the L2 SNR determinations and by the problem of the sign ambiguity in the estimated multipath corrections in common high-precision geodetic observations [*Scappuzzo*, 1997; *Bilich et al.*, 2002, 2003; T. Herring, personal communication, 2004]. Other related methods make use of the carrier-to-noise power-density ratio information [e.g., *Brunner et al.*, 1999] to assign lower weights to phase observations affected by multipath when estimating geodetic parameters of interest. Although improvements in site position estimates are quite significant, this method does not model multipath or scattering but, in essence, provides a criterion for rejecting (downweighting) observations presumably contaminated by these errors.

[5] Measurement of GPS antenna phase patterns [*Schupler et al.*, 1994; *Schupler and Clark*, 2001] in an anechoic chamber indicate contributions of up to 20 mm, varying with azimuth and elevation angle. However, these measurements are of limited use because of the near-field nature of the problem [*Elósegui et al.*, 1995]. Deployed in the field, GPS antennas are usually mounted directly on larger structures that electromagnetically couple to the antenna, effectively modifying the phase pattern. Some improvements in geodetic parameter estimates have been noted using corrections based on anechoic chamber measurements [*Meertens et al.*, 1996], but such corrections cannot deal with site-dependent contributions. This same problem applies to the mapping of phase-center variations in the field using a robot that rotates the antenna about several axes [*Wübbena et al.*, 2000]. Indeed, the robot itself may become coupled electromagnetically to the GPS antenna during calibration.

[6] Instrumental approaches based on multielement GPS antenna arrays have also been designed to reduce multipath errors [e.g., *Counselman*, 1999] and have met with varying degrees of success. Additional instrumental approaches to mitigate multipath effects include signal processing techniques in the receiver itself. Some of these methods, based on narrow-correlator techniques, are effective in mitigating multipath errors caused by objects in the far field that are delayed by tens of meters with respect to the direct signal, but do not solve the problem of near-field multipath (i.e., scattering) [e.g., *Weill*, 2002], whose effect on high-precision GPS geodesy is worse [*Elósegui et al.*, 1995].

[7] An entirely ad hoc approach capitalizes on the assumed repeatability of these effects [e.g., *Genrich and Bock*, 1992; *Wdowinski et al.*, 1997]. The satellites in the GPS constellation are in pseudosynchronous orbits, with the topocentric satellite positions repeating every sidereal day. *Bock et al.* [2000] have filtered out the common mode effects of signal multipath using the sidereal repetition. Although this method is very effective at reducing postfit phase residuals and is computationally efficient, it also can filter out other signals that have sidereal periods. Another disadvantage of this correction is that it is based on postprocessing analysis. Thus multipath errors at each individual site might have already propagated into the estimates of other parameters, especially the estimates of the vertical site position and atmospheric propagation delay.

[8] Despite these studies, much remains uncertain about these important error sources, including their variations among sites and their variability over time. This latter effect can be expected since sites physically change with time, both seasonally (e.g., foliage changes)

and on shorter timescales (moisture, precipitation, and equipment changes). What is required is an in situ method for measuring these effects. With this goal, we have developed an Antenna and Multipath Calibration System (AMCS) that uses a relatively high-gain parabolic antenna to calibrate a GPS antenna at a site. The parabolic antenna is directional and thus suffers negligibly from phase-center variations and multipath. In this article we describe the design and operational aspects of the AMCS, and present the results of preliminary tests designed to assess its accuracy.

2. AMCS Theory

[9] We assume that we have two GPS receivers, each fed by a different antenna and recording the carrier beat phase for either or both of the GPS carrier frequencies, L1 and L2. If the baseline vector, $\vec{b}$, separating the two antennas is short (i.e., $b/\rho \ll 1$, where ρ is the topocentric satellite distance), then the single-difference phase observable $\Delta\phi$ formed by differencing the phase measurements from the two receivers for a common epoch and satellite is given in cycles by

$$\Delta\phi(t) \simeq \frac{f}{c}\hat{s} \cdot \vec{b} + \frac{f}{c}\dot{\rho}(t)\Delta T + \Delta\phi_\circ + \Delta\phi_I(t) + \Delta\phi_N(t) \\ + \Delta\phi_A(t) + \Delta\phi_M(t) + \Delta\epsilon(t), \qquad (1)$$

where f is frequency, c is the speed of light, $\hat{s}$ is the topocentric satellite unit vector (implicitly a function of time), $\dot{\rho}$ is the topocentric satellite distance rate, ΔT is the "clock synchronization" error (i.e., the difference between the "time tags" for the two receivers; see below for typical values), and $\Delta\phi_\circ$ is a phase offset that incorporates cycle ambiguities. The next four terms in equation (1) represent differences between the contributions due to the ionosphere (subscript I), neutral atmosphere (N), antenna phase-center variations (A), and multipath (M), and the last term represents the difference in measurement noise. (Note that the M term includes both multipath and scattering effects, which represent, respectively, the far- and near-field manifestation of the same physical phenomenon [e.g., Elósegui et al., 1995].) If the clock synchronization error changes significantly over the period to be considered, there is an additional term $f\Delta T$ that we have assumed is constant and incorporated into $\Delta\phi_\circ$.

[10] As we will see below, the AMCS operates in two distinct modes. In the primary calibration mode (called "AMCS mode") one of the antennas is a GPS antenna to be calibrated in situ (the "test antenna"), and the other antenna is an antenna designed so that the contributions from phase-center variations, multipath and scattering are effectively zero (see below). The ionospheric contribution $\Delta\phi_I$ is also negligible (≤ 0.2 mm at $10°$ elevation

angle at both L1 and L2 wavelengths when b is less than 40 m). The contribution of the neutral atmosphere $\Delta\phi_N$, on the other hand, is not negligible because the height difference between the antennae may be significant (see below). For the AMCS mode, equation (1) can thus be written

$$\Delta\phi_{\text{AMCS}}(t) \simeq \frac{f}{c}\hat{s} \cdot \vec{b} + \frac{f}{c}\dot{\rho}(t)\Delta T + \Delta\phi_\circ + \Delta\phi_N(t) \\ + \phi_A^T(t) + \phi_M^T(t) + \Delta\epsilon(t), \qquad (2)$$

where the superscript T indicates the contribution from the test antenna only and, thus, the difference symbol (Δ) for the A and M terms has been dropped. The term $\Delta\phi_N$ is, even at low elevation angles, rather insensitive both to accurate knowledge of the height difference between the two antennae and to variations in refractivity. The insensitivity to these parameters makes it then possible to determine $\Delta\phi_N$ accurately and subtract that contribution from equation (2).

[11] In the second mode of operation, the test antenna is used to feed both GPS receivers simultaneously by means of a splitter (see below). In this mode (called the "zero-baseline mode" or "ZBL mode") contributions from propagation media, antenna phase-center variations, and multipath are equal and cancel, and $\vec{b} = 0$. The ZBL mode observation equation thus reduces to

$$\Delta\phi_{\text{ZBL}}(t) \simeq \frac{f}{c}\dot{\rho}(t)\Delta T + \Delta\phi_\circ + \Delta\epsilon(t). \qquad (3)$$

[12] To achieve the quality of negligible phase-center and multipath errors, the AMCS employs a high-gain, fully steerable, 3-m diameter parabolic reflector. This antenna has a beamwidth (full width at half maximum, FWHM) of $5.5°$ at the L1 frequency. The first sidelobes at the L1 frequency extend out to $\sim 13°$ and reject signals at the level of $20-30$ dB at this point. Beyond the first sidelobe, signals are rejected at the level of ~ 34 dB or greater. For comparison, a typical GPS antenna of Dorne-Margolin choke ring design receiving a primary GPS signal at $20°$ elevation angle rejects reflected signals arriving from $-20°$ elevation angle at a level of only ~ 10 dB [e.g., Tranquilla et al., 1994]. (Here and below, brand names are used for identification purposes only.) Thus the AMCS antenna multipath signal rejection is ~ 16 times greater (voltage) than that of the Dorne-Margolin design antenna, for a phase contribution less than 1 mm for most conditions.

[13] As is described in more detail below, ZBL mode observations are used to determine the unknown parameters ΔT and $\Delta\phi_\circ$ in equation (3). (There is one value of $\Delta\phi_\circ$ for each satellite.) With these parameter values known, the AMCS mode observations can then be used
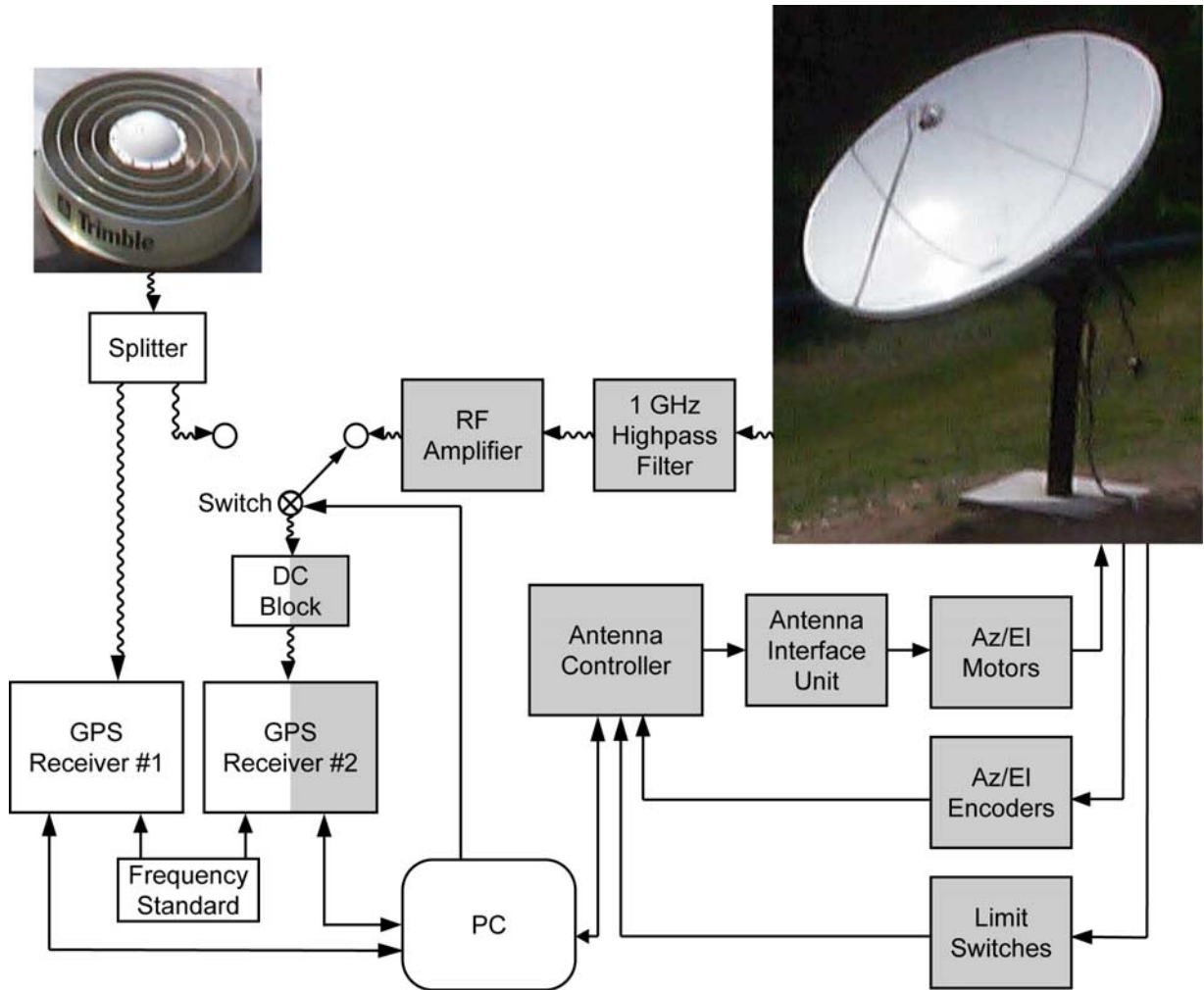
Figure 1. Block diagram of the Antenna and Multipath Calibration System (AMCS), with switch shown in AMCS mode (see text). Insets are photographs of (left) the test antenna and (right) the parabolic antenna. The GPS signal received by each antenna feeds one of the two GPS receivers, which are both driven by the same external frequency standard. A PC controls the receivers, the switching between operating modes, and the azimuth and elevation angle motors and encoders of the parabolic antenna. Shading highlights components directly related to the parabolic antenna. GPS receiver number 2 is fed with signals coming from either the parabolic antenna or the test antenna and is thus half shaded. Wavy lines represent GPS signal path, and thin lines represent communication and control paths, with arrows indicating direction.

to determine the combined antenna multipath contribution $\phi_A^T + \phi_M^T$ from equation (2).

3. Prototype AMCS Design and Implementation

[14] We constructed a prototype AMCS on the grounds of Haystack Observatory in Westford, Massachusetts. Although ultimately a portable system will be required

to calibrate individual sites, for the prototype AMCS the receiver and electronics were housed in a trailer and the antenna was set in concrete to minimize errors associated with mechanical motions.

[15] The prototype AMCS uses two Trimble 4000 SSI receivers. An RF switch and DC block enable changing between AMCS mode and ZBL mode (Figure 1). For ZBL mode observations, a signal splitter is connected to the test antenna output so that the received signal can be fed simultaneously to the two receivers. A PC controls

mode switching as well as operation of the AMCS antenna, acquisition of AMCS antenna position information, and acquisition of GPS data.

[16] A 5-MHz signal from a common oscillator serves as the frequency standard for both GPS receivers. Since a hydrogen maser (Allan standard deviation of 10^{-14} s·s^{-1} for periods between 10 and 10^5 s) was readily available at Haystack Observatory, we used it, although in principle a less stable oscillator would suffice.

[17] The 3-m diameter hydroformed aluminum parabolic reflector antenna (Andersen Manufacturing Inc.) has quad feed support rods and dual azimuth elevation angle drives. A left circularly polarized L band antenna feed (Microwave Engineering Corporation) is mounted at the prime focus. The entire drive-reflector assembly is mounted on an 8-inch ($\sim$0.2 m) diameter, 10-foot ($\sim$3 m) long steel pipe, $\sim$1 m of which is anchored in a 1.2-m cube of concrete. (Non-SI units are given when they correspond to standard manufacturer specifications and for identification purposes.) Two $0.25 \times 3 \times 2$-inch ($\sim 6 \times 76 \times 50$ mm) tabs were attached to the pipe near the very bottom for (azimuthal) rotational stability.

[18] The antenna can be pointed within the ranges $7°$–$357°$ (azimuth) and $5°$–$87°$ (elevation angle). A 36-inch ($\sim$0.9-m) ball screw (Thomson Saginaw Performance Pak Linear Actuator) was installed to position the parabolic antenna to a desired elevation angle. A chain drive is used to move the antenna in the azimuth direction. Tracking precision is $0.5°$ in azimuth and $\sim 0.1°$ in elevation angle. The azimuth drive has a speed of $2°$ per second and the elevation drive a speed of $0.8°$ per second. To control antenna pointing, a satellite antenna controller model RC2500 (Research Concepts, Inc.) is used. Power to the DC motor drives was provided by two modified Smart Booster II antenna interface units (Research Concepts, Inc.), which were controlled by the RC2500 controller. We installed absolute resolvers to sense antenna angular position with $6'$–$7'$ resolution, and mechanical limit switches to prevent over-rotation.

[19] A phase-stabilized cable (Andrew FSJ1-50A) feeds the signals from the antennas to the GPS receivers. The attenuation of the signal at L band is $\sim$7 dB per 100 ft ($\sim$0.2 dB per m) at an ambient temperature of 24°C. The total length of cable from the feed of the parabolic antenna to the receiver is $\sim$30 m, and the temperature sensitivity of the electrical length varies between -7 and $+9$ μm per meter per degree Celsius for temperatures between $-30°$ and $+40°$C. We reduced the effects of temperature-induced cable-length electrical variations by equalizing the lengths of both receiver cables exposed to the ambient temperature. We further reduced temperature-related errors by placing the GPS receivers in the trailer, which is a temperature-moderated environment.

[20] The LabVIEW™ graphical user interface is used to operate the AMCS either automatically or manually. The interface handles switching between ZBL and AMCS modes, selecting satellites to observe, pointing the antenna, and acquiring data (Figure 2). The LabVIEW™ routines also control the communication between the PC and the GPS receivers and download the satellite ephemerides and phase data. Multiple receiver channels can be assigned to specific satellites. The LabVIEW™ routines are supported by a set of MATLAB™ routines that handle the more computationally intensive tasks, such as calculation of topocentric satellite positions, performing least-squares solution for synchronization errors, and calibration solutions. We can remotely operate the AMCS via an Internet connection. For safety reasons, a digital video camera was connected to the PC so that one can remotely observe the antenna to insure that it is safe to move.

4. ZBL Mode Results

[21] As we discussed above, the ZBL mode is used to estimate the receiver synchronization error ΔT and phase offset $\Delta \phi_\circ$ in equations (1)–(3). It also serves to assess the precision of the difference phase observable in our system. From equation (3) it can be seen that the ΔT and $\Delta \phi_\circ$ parameters can be easily determined from a linear least-squares fit to the ZBL mode single-difference phase observables, if $\dot{\rho}$ is sufficiently well known. This condition is easy to achieve using the satellite ephemerides broadcast by the GPS satellites and an approximate position calculated by the GPS receiver itself.

[22] We have adopted a scheme whereby the AMCS is operated in ZBL mode for 10 min, alternating with data acquisition in AMCS mode for 15 min. We have set the data sampling period to 10 s. (Different switching cycles and sampling rates are also possible and were tried. The scheduling parameters we used were chosen to balance computer processing load and the rate of variations of the multipath and phase-center terms in equation (2); see below.) During each 10-min ZBL mode scan, ΔT is assumed to be constant. Typical values for this parameter are several tenths of milliseconds, with variations of only a few microseconds over several hours. A typical uncertainty for the ΔT parameter is 1.5 μs.

[23] Figure 3 shows an example of ZBL mode residuals to a least-squares fit of difference phase observations of five GPS satellites for a 10 min scan. In this example and several others below, the phase is measured in units of equivalent path length at the relevant carrier frequency. (The results presented in this paper are all based on L1 because it is more precise than L2. The next phase of our study will also include tests using L2.) The
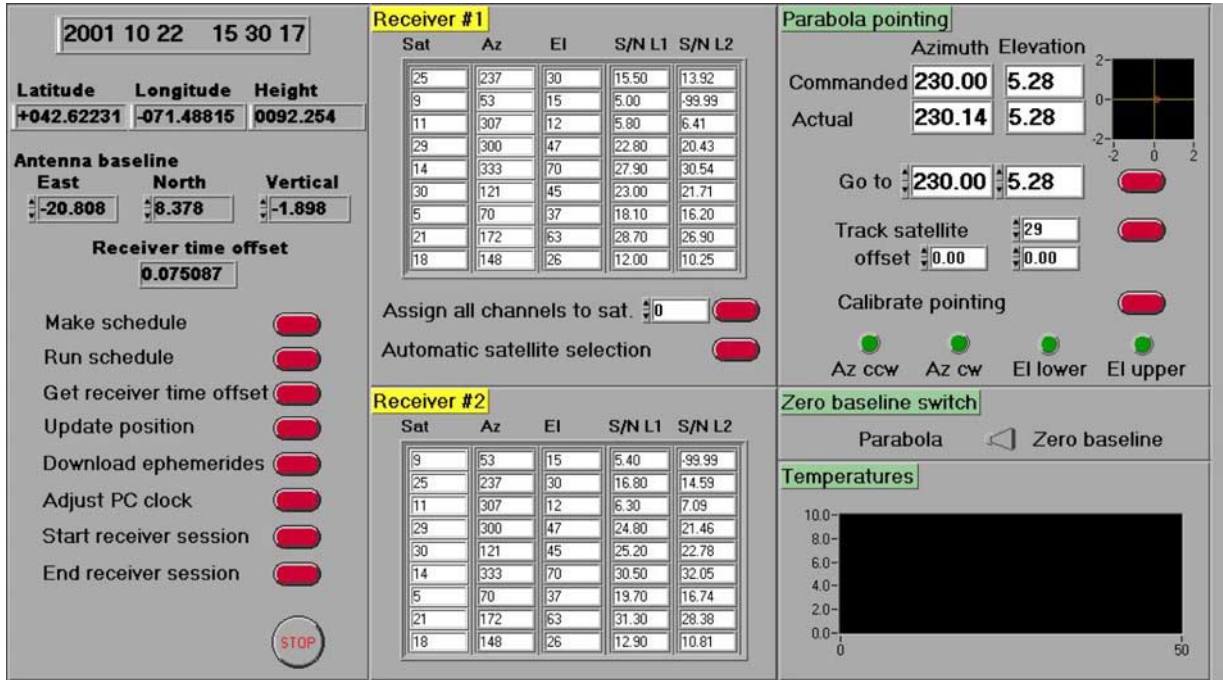
Figure 2. Example of a control-and-report graphical user interface window of the AMCS showing observing epoch, receiver clock synchronization, site and satellite parameter values, antenna pointing direction, and operating mode. The information displayed is refreshed at every sampling epoch, which the user can select, or faster when, for example, the parabolic antenna is slewing between different satellite pointing directions.

solution was obtained assuming equal weight for all observations, regardless of GPS satellite (indicated by the pseudorandom noise (PRN) code number in Figure 3) or elevation angle. (In fact, the observational noise should vary with SNR, which varies slightly with elevation angle, and with other conditions such as multipath.) Again assuming equal weights, the root-mean-square (RMS) residual from the ZBL mode scan is a measure of the observational uncertainty. The RMS residual in Figure 3a is 0.5 mm. We found that the typical RMS residual from the ZBL mode runs is $0.5-0.6$ mm.

[24] In Figure 3a one can observe systematic variations of the residuals that are of amplitude ∼0.5 mm. We ascribe these variations to temporal variations in ΔT, which is common to all satellites for each epoch. (In equation (3), a constant term $f\Delta T$ was lumped into $\Delta\phi_\circ$, but temporal variations in $f\Delta T$ were neglected.) Figure 3b shows the mean value of the residuals for each epoch, which range between ±0.9 mm. The RMS variation of these mean values is 0.4 mm, which corresponds to a value for the RMS variation of ΔT of 1.3 ps. The residuals of the ZBL phase residuals of each satellite relative to the estimated mean values are shown in

Figure 3c. The RMS residuals are 0.2 mm for PRNs 2, 4, and 7, 0.4 mm for PRN 9, and 0.3 mm for PRN 20. The variation in RMS residuals is reasonably explained by the difference in elevation angles of the satellites (PRN 2: 54°; 4: 52°; 7: 77°; 9: 17°; 20: 40°). We thus conclude that the contribution due to the picosecond-level (submillimeter) variations in ΔT dominates the residuals from the ZBL mode runs. Although equation (3) could include a time-varying ΔT parameter to estimate the temporal variations in the ZBL mode, it is not useful to do so because those estimates could not then be applied to the AMCS mode observations. Therefore the AMCS calibration will consist of the combined antenna-multipath contributions $\phi_A^T + \phi_M^T$, plus a submillimeter-level (∼0.4 mm RMS) contribution due to temporal variations in ΔT, plus a random noise component (∼0.2 mm or more, depending on elevation angle).

5. Calibration of Antenna and Multipath Errors

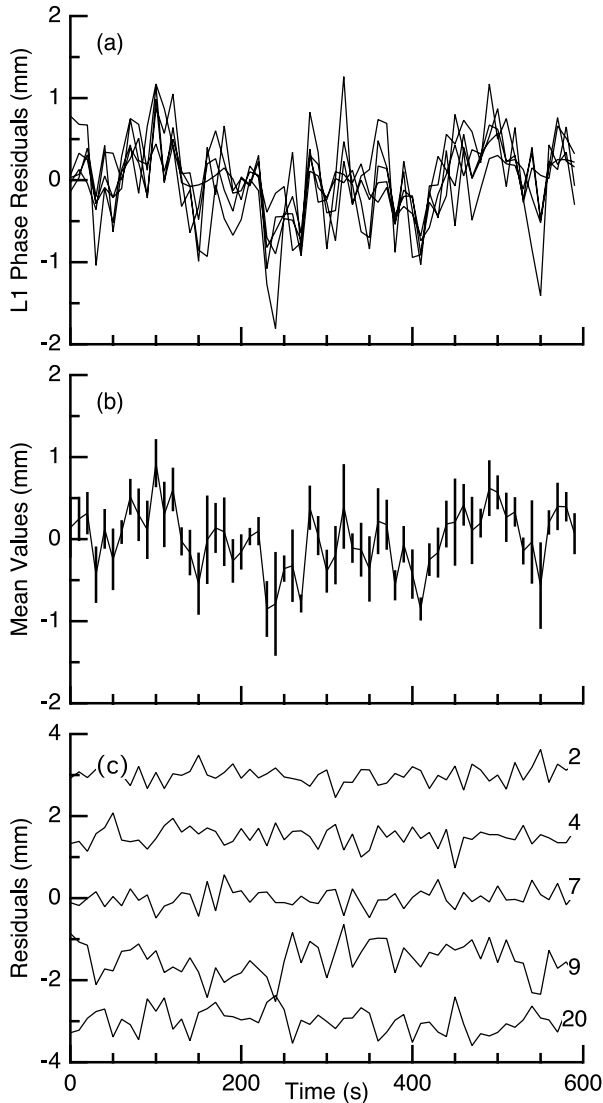[25] The measurements presented in this section are intended to verify and assess the design and operation of

Figure 3. Example of (a) L1 postfit difference-phase residuals, (b) mean residual value at each epoch, and (c) residuals of Figure 3a to the mean value estimates of Figure 3b from a 10-min ZBL mode scan. Each trace represents a different GPS satellite. The error bars in Figure 3b are the RMS residual at each epoch around its mean values. The trace in Figure 3b represents variation in ΔT. The traces in Figure 3c are the postfit residuals with ΔT variations removed and represent random measurement noise that varied with elevation angle. Numbers on the right-hand side of Figure 3c represent satellite pseudorandom noise (PRN) code number. Times are referenced to the first epoch, which is at 1429:13 UTC on 17 May 2001. Each trace in Figure 3c is vertically offset by a multiple of 1.5 mm for clarity. Note the difference in the vertical scale between Figures 3a and 3b and Figure 3c.

the AMCS. For the "test antenna" to be calibrated we used a standard geodetic Dorne-Margolin choke ring antenna manufactured by Trimble. We used a modified form of the AMCS mode observable equation (2) that takes into account the offset between the phase reference of the AMCS feed and the intersection of axes:

$$\Delta\phi_{\mathrm{AMCS}}(t) \simeq \frac{f}{c}\hat{s}\cdot\vec{b} + \frac{f}{c}\dot{\rho}(t)\Delta T + \Delta\phi_{\circ} + \Delta\phi_N(t)$$
$$+ \phi_A^T(t) + \phi_M^T(t) + C\cos\varepsilon + \Delta\epsilon(t), \qquad (4)$$

where ε is the elevation angle. The value of C, the axis offset, for the AMCS antenna, 0.250 m, was determined with a ruler calibrated to a precision of 1 mm. The neutral atmospheric contribution was calculated using

$$\Delta\phi_N(t) = -10^{-6}\, N_{sl}\, e^{-z/H}\, m(\varepsilon(t))\, \Delta Z, \qquad (5)$$

where N_{sl} is a value adopted for the radio refractivity at sea level, z is the altitude of the test site, H the atmospheric-scale height, m is the mapping function [e.g., *Davis et al.*, 1985], and ΔZ is the difference in ellipsoidal elevations for the AMCS and test antennae (in the sense AMCS minus test). We adopted standard values of 300 N for N_{sl} and 8 km for H, and used a "cosecant law" for m. For example, for an elevation angle of 5°, the neutral atmospheric contribution $\Delta\phi_N$ ranges between 3.4 and 3.0 mm per meter of ΔZ for respective site altitudes between 0 and 1000 m above sea level. Because this contribution is insensitive to reasonable errors in all the parameters (vertical distance between sites, site altitude, temporal variations of sea-level refractivity, and scale height parameter), it is possible to determine it accurately (submillimeter level) and subtract it from equation (4).

[26] To estimate $\phi_A^T + \phi_M^T$ in equation (4), the effects of the baseline geometry (first term on the right-hand side) must be accounted for. For our tests, the baseline vector was determined by a combination of conventional surveying and estimation using GPS data. The conventional surveying was done using the standard antenna reference point on the test antenna and a physical mark in the parabolic antenna. In the future, we plan to automate this function as a part of the setup procedure for the mobile AMCS. However, it is clear that, if GPS data are used for this purpose, multipath errors can easily propagate into the baseline-coordinate parameters which, in turn, will propagate into the maps for multipath and antenna calibration. Thus the multipath and antenna calibration can create a new reference location for the calibrated GPS antenna that is associated with a specific calibration map. This is true of all such calibrations, however, and is not unique to the AMCS.

[27] Therefore an accurate determination of the baseline vector by a means other than GPS, for example

conventional surveying techniques, is required for the ultimate goal of measuring the in situ phase pattern, and the accuracy of the phase calibrations will be limited by the accuracy of such survey. For the present investigation, however, the variation in phase due to a baseline error contributes only a slow, approximately linear change of about 0.5 mm per millimeter of baseline error (over the few degree range of elevation and for low elevation angles; see below).

[28] Since we have no "ground truth" multipath map with which to compare our determinations, we designed our tests to take advantage of what we understand to be true regarding multipath: that multipath and antenna phase errors should, to the extent that the electromagnetic conditions within the site environment remain constant, be repeatable; that multipath conditions are worse for environments with more metal reflectors nearby the antenna; and that the phase multipath errors and antenna phase variations are generally greater for lower elevation angles.

5.1. Source Direction and Time-Repeatability Experiments

[29] We performed various series of experiments to assess the ability of the AMCS to calibrate GPS antenna-dependent errors. In all the experiments the GPS test antenna was mounted on a boom jutting out of a corner of a flat roof of a trailer located on the edge of a parking lot. The trailer, which served to house the AMCS receivers and other electronics, is about 9 m long by 2.5 m wide by 3 m high. Its roof surfacing is metal painted. The L1 reference point of the GPS test antenna was at a horizontal distance of 22 m from the parabolic antenna along an azimuth of 112, and 2 m above it. Each experiment consisted of an alternating sequence of about 10 min of measurements with the system operating in ZBL mode followed by about 15 min of measurements with the system operating in AMCS mode, that is, while the parabolic antenna was tracking a specific GPS satellite. As described above, the ZBL mode measurements are used to estimate ΔT and $\Delta\phi_\circ$ in equation (3), and these estimates are then used with the AMCS mode measurements to determine $\phi_A^T + \phi_M^T$ in equation (4). The values $\phi_A^T + \phi_M^T$ represent the combined calibration of antenna and multipath effects for the test antenna. Because of the expected repeatability of these errors with sidereal day, we repeated the same experiment at the same sidereal time over several consecutive days.

[30] In our initial experiments we constructed "full-sky maps" of the AMCS phase and multipath contributions, i.e., calibration maps for the sky covered by the topocentric path of the complete constellation of GPS satellites over 24 hours. Because these maps appeared extremely noisy relative to the typical uncer-
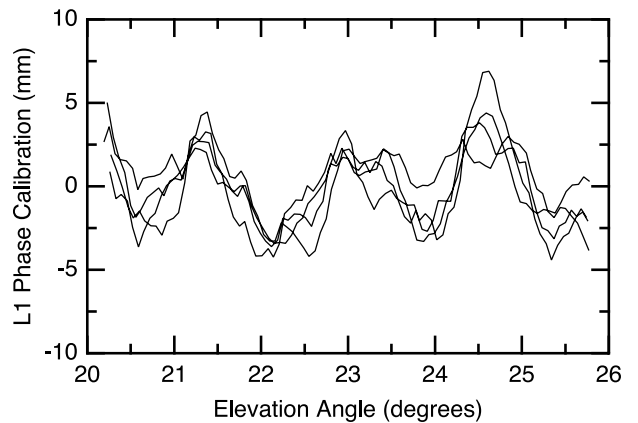

Figure 4. Example of estimates of L1 phase calibrations from 15-min AMCS mode scans from PRN 1 for four consecutive days.

tainty from the ZBL mode measurements and the expected uncertainty from the AMCS mode measurements, we focused on experiments of more limited sky coverage. Figure 4 shows L1 phase calibrations (i.e., $\phi_A^T + \phi_M^T$) for one of such a series of experiments as a function of satellite elevation angle. The phase calibrations are for GPS satellite PRN 1 and are sampled at 10 s intervals on four consecutive days, from 18–21 November 2001. During the approximately 15 min duration of each scan, the elevation angle varied by 6° (20°–26°), while the azimuth angle varied only by 1° (310°–311°). The residuals in Figure 4 have been smoothed with a Gaussian window with a FWHM of 50 s to reduce the scatter due to the small, ps-level variations in ΔT discussed above. A salient feature of this figure is the rapid variability of the estimated phase calibrations, with variations that amount to about 10 mm of phase peak to peak over a fairly small range of elevation angles. Moreover, these features display a high degree of repeatability over the four consecutive days. Repeatability with signal direction is a key characteristic of both multipath and phase-center errors. The differences among phases on different days are significantly larger than the 0.5–0.6 mm observational uncertainty determined from the ZBL mode, and are unlikely to be simply noise. Instead, they might result from short-term (daily) variations in the electromagnetic environment of the GPS antenna due to varying atmospheric or ground conditions.

[31] We performed similar series of experiments using the same experimental setup throughout the Fall of 2001 with this same PRN 1 satellite at other elevation and azimuth angles and with other GPS satellites covering a wide range of elevation and azimuth angles. The results were consistent with those presented in Figure 4. In

particular, we found that the estimated calibration signals generally repeated with satellite position and sidereal time but that the day-to-day differences could be at the millimeter level. We also found that small changes in satellite position could cause large signal variations and that the signature of the variations with elevation angle could have a "wavelength" of about $1-2°$ of elevation angle. Also, the amplitudes of the variation were generally larger at low ($25°$) elevation angles, with typical values that ranged between 4 and 7 mm, whereas the amplitude for experiments performed at higher ($25°$) elevation angles ranged between 1 and 2 mm.

[32] The signature of the results just presented is characteristic of multipath and scattering and suggests very strongly that the variations measured are due to antenna-dependent effects. We further investigate this hypothesis in the next section.

5.2. Multiple Test Antenna Experiments

[33] The results of the tests described in the previous section indicated that we were able to observe patterns of multipath and scattering plus (probably smaller) antenna errors for the test antenna (i.e., $\phi_A^T + \phi_M^T$) that repeated with signal (i.e., satellite) direction and sidereal time. In making the inference that the observed phase "signal" was indeed $\phi_A^T + \phi_M^T$, we assumed that the contribution of any potential AMCS error is negligible, but these tests by themselves were not enough to conclude that this assumption was correct. To rule out that the source of the repeatable phase variations was not the AMCS itself, we made measurements with a second GPS test antenna. This second test antenna was placed on a platform that was electromagnetically shielded from the test antenna by means of microwave absorber and sat above the surrounding tree line. This test antenna was at a horizontal distance of 31 m from the parabolic antenna along an azimuth of $131°$, and 4 m above. Because the location is relatively free from local reflectors, we would expect to see a lower multipath signal at this site. We then made observations from both test antennas, alternating between them on successive days. If the phase variations we observed in the previous tests were associated with the AMCS itself, we would see little difference between the measurements with the different test antennas.

[34] For these series of tests, we collected data for seven days in February 2002. The test antenna 1 (the same antenna in the same location as the previous tests) was used for two days (16 and 18 February) and test antenna 2, in the low-multipath environment, was used for five days (13, 15, 17, 19, and 20 February). As in the previous tests, the parabolic antenna tracked each GPS satellite for 15 min, preceded by 10 min of ZBL.

[35] Figure 5 shows the L1 phase calibrations for each test antenna, and for several different signal directions. Figures 5a−5c display the results for test antenna 1, and Figures 5d−5f for 2. Figure 5 is laid out so that in comparing vertical pairs of panels, e.g., Figures 5a and 5d, one is comparing results for the same direction and sidereal time. Figures 5a and 5d and Figures 5b and 5e are for different GPS satellites (PRN 30 and PRN 5, respectively) that happen to appear in the same location of the sky at different times of the day. The azimuth angles for a given elevation angle differ by $\sim 1°$ between pairs Figures 5a and 5d and Figures 5b and 5e. Figures 5c and 5f are also for satellite PRN 5, and the azimuth angles between Figures 5b and 5e and Figures 5c and 5f differ by $\sim 14°$. The traces in Figures 5d−5f for each of the days on which test antenna 2 was used are staggered by 6 mm for clarity.

[36] A number of observations regarding this test can be made. First, the low-elevation angle results for the high-multipath environment (Figures 5a and 5b) repeat very well, as with the previous tests. The calibration also varies greatly with elevation angle, a result seen in the previous test (Figure 4). Figures 5a and 5b both have "maxima" at about the same elevation angles. However, there are significant differences between these panels as well. (Note that the horizontal scales differ also.) The rapid variation of the calibration with elevation angle indicates that a difference of $1°$ or so can be significant. It is plausible, then, that the difference between Figures 5a and 5b is due to the azimuth angle difference.

[37] Figure 5c shows the calibration for much higher elevation angles. Although some of the main features of the curves for the two days of Figure 5c agree well, there appears to be a greater difference between these two curves than for the curves of Figures 5a and 5b. In part, this is a visual artifact of the large variation of the calibrations in Figures 5a and 5b. In Figures 5a−5c the differences between the two days can reach several millimeters. The pairs of curves in Figures 5a−5c all have differences with a minimum to maximum range of ~ 6 mm.

[38] The elevation angle-dependent variations in the curves from the expected low multipath environment, Figures 5d−5f, are in fact smaller by about a factor of two than those of Figures 5a−5c. Consistent with Figures 5a−5c also is the observation that the variations at the higher elevation angles in Figure 5f are smaller than those of Figures 5d and 5e. Similarities can be seen in many of the features of the curves obtained on the different days in Figures 5d−5f, but differences can be seen also. For example, in Figure 5e the calibration shows no large feature between $15°$ and $16°$ for days 13 and 15. There is a large (6 mm) negative feature in this range for days 17 and 19,
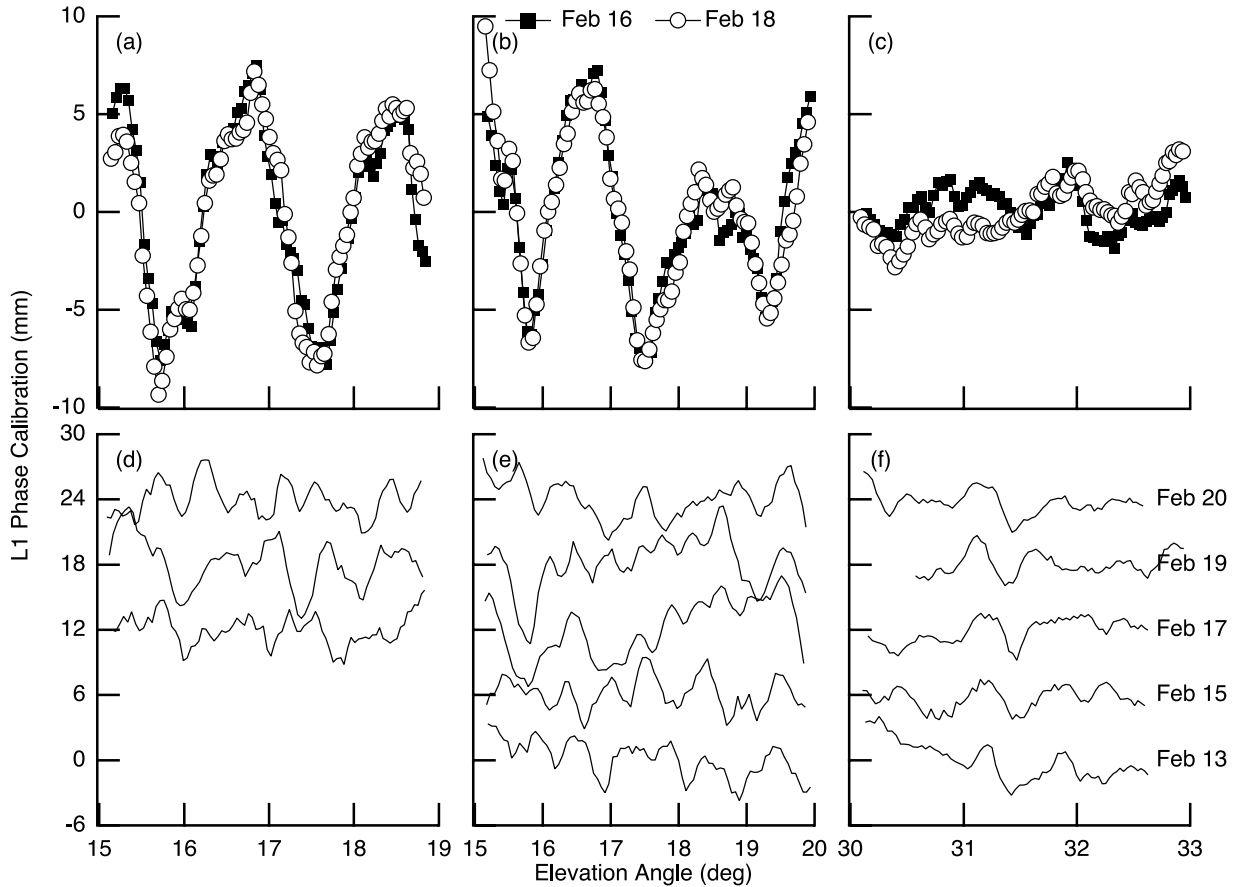
Figure 5. Estimates of L1 phase calibrations from 15-min AMCS mode scans. (a)–(c) GPS test antenna 1 (see text) on 16 and 18 February 2002. (d)–(f) GPS test antenna 2 on 13, 15, 17, 19, and 20 February 2002. In Figures 5a and 5d, PRN 30 was observed. In Figures 5b, 5c, 5e, and 5f, PRN 5 was observed. The traces in Figures 5d–5f are offset by 6 mm for clarity. Note the difference in the vertical scale between Figures 5a–5c and Figures 5d–5f.

however. On day 20, the feature has either disappeared or has decreased in size significantly. On the other hand, in Figure 5f the feature between 31° and 31.5° persists for all five days.

[39] Our interpretation of this test is that the main features of the AMCS phase calibration, first seen in the previous section, are indeed associated with combined phase multipath, scattering, and antenna-phase errors since they have the following features: (1) for a given test antenna the features generally repeat with satellite position at the same sidereal time on different days; (2) the largest features agree well for similar satellite positions for different satellites, even when these similar satellite positions occur at different sidereal times; (3) the phase calibration variations are smaller for greater elevation angles; and (4) the phase calibration variations are smaller for a test antenna in an environment that

we surmised beforehand would in fact induce lower multipath.

[40] We therefore interpret differences in calibration with position (i.e., Figures 5a and 5d versus Figures 5b and 5e) as real differences in calibration, and differences between days as differences in calibration due to changes in environment. Changes in the electromagnetic properties of the environment can be caused, for example, by precipitation or by melting or freezing of snow and ice. Previous work on multipath and scattering [e.g., *Elósegui et al.*, 1995] demonstrated that multipath phase depends on the value of the attenuation of the signal on reflection. The presence of varying amounts of surface water, snow, or ice may affect this value [e.g., *Jaldehag et al.*, 1996]. Between 13 and 20 February 2002, previously accumulated snow was present and the temperature oscillated around 0°C, and on day 17 there was rain and freezing

fog. (These data were obtained at http://www.noaa.gov/.) If these varying conditions were responsible for the changes in multipath and scattering, then a lower limit of 3–5 mm can be inferred for environmental effects.

[41] The statistics of the multiday experiments yield important information regarding the temporal variability of the site multipath as well as the performance of the AMCS. For example, we used the five curves in Figure 5f to form an average multipath curve. The residual of the multipath curve measured on a particular day to the average multipath may then be calculated. The RMS value of this "multipath variation," which represents the combined effect of multipath and AMCS noise, was 0.4 mm on 20 February, 0.7–0.8 mm on 15, 17, and 19 February, and 1.0 mm on 13 February. The AMCS "system noise" for this range of elevation angles, based on the results of section 4, should be 0.4–0.5 mm. The increased noise apparent on all days but 20 February may be an indication of multipath variability for this site at this elevation angle range, increased variable AMCS system noise of unidentified origin, or a combination of these two effects. The overall RMS residual of these curves from their mean, clearly reflecting the domination of the larger values, is 0.8 mm. If the multipath variability were zero, this would represent a value for the AMCS "system noise." Using a value for the baseline AMCS system noise of 0.4–0.5 mm, the multipath variability for this site and elevation-angle range would be 0.6–0.7 mm. At this point, we cannot definitively separate these effects, but given the variability of environmental conditions and their correlation with phase variability described above, there is no reason to suspect that the AMCS is, in AMCS mode, performing at a level worse than that characterized by the ZBL analysis.

6. Summary and Discussion

[42] We constructed the AMCS along a design that had never been attempted since we wished to obtain in situ site corrections. We therefore began our study by performing "zero baseline" measurements intended to quantify the receiver noise. These ZBL measurements indicated that we could expect phase difference measurements with an uncertainty of ∼0.5 mm (L1). This value is dominated by the stability of the receiver clock differences, which were ∼1–2 ps RMS. (On the basis of a multiparameter benchmark comparison we performed with various standard geodetic receiver brands available at the time, we did not expect other receivers to have better clock stability than the Trimble SSI receivers we used; this situation will be revisited since receivers with improved technology are now available.) These studies thus placed a lower limit on the noise that we could expect from the AMCS.

[43] When we used the AMCS to construct full-sky maps of the antenna phase and multipath contributions $(\phi_A^T + \phi_M^T)$, these appeared to be extremely noisy, with RMS phase variations of ∼5 mm or more, i.e., a factor of at least ten greater than the system noise. Allowing for the possibility of an AMCS system error, we therefore designed experiments of more limited sky coverage, which are described here. These experiments, very time-intensive to perform and analyze in detail, cover only very small arcs (few degrees) of a GPS satellite path in the sky. From the experiments reported here we concluded that the observed quasi-sinusoidal variations were in fact real variations in $\phi_A^T + \phi_M^T$, as were the variations observed in the preliminary sky maps. Although we cannot unambiguously separate multipath and scattering from antenna phase-center effects, it seems unlikely that such large variations over such small angles are due to the latter [e.g., *Schupler and Clark*, 2001]. We also observed day-to-day millimeter-level changes in the calibration that we hypothesize are changes in multipath caused by changes in the electromagnetic environment associated with, e.g., weather. Further studies are needed to assess this hypothesis.

[44] The variations in the antenna phase and multipath calibration across a spatially small area of the sky have not previously been reported. This is probably due to the approaches used, which tend to average or poorly sample over so small an area of the sky. *Hurst and Bar-Sever* [1998] and *Reichert* [1999], for example, average their results into patches that are $1° \times 1°$. Methods that depend on residual averaging [e.g., *Genrich and Bock*, 1992] derive their spatial resolution from their temporal sampling. Common sampling periods for geodetic GPS are 30 s (leading to changes in elevation angle of ∼0.5° between samples) or 300 s (5°). Fitting low-order spherical harmonics [*Reichert*, 1999] also ignores these variations, which are effectively high order and degree. Some of these methods even assume azimuthal symmetry and hence average all phase measurements over bands of elevation angle without consideration of azimuth angle. Unlike these approaches, the AMCS is, by construction, an absolute calibrator of each individual phase measurement and, independently, for each GPS wavelength.

[45] Corrections for site-dependent errors are incorporated in GPS data processing by means of phase calibration maps [*Hurst and Bar-Sever*, 1998]. These are direction-dependent calibrations that are applied to the modeled GPS phase observations to correct for these errors. Construction of such maps is the ultimate goal for the AMCS. Prior to achieving that goal, however, we intend to use the AMCS to study the best approach to calibration, to assess the observed variations, and to quantify the effects of environment and weather. Moreover, as we better understand these effects and how they may vary with topocentric direction, time, and site

location and layout, we will be able to obtain a better understanding of their effect on various geodetic parameters. The next phase of our study, therefore, will be to construct a portable AMCS and to streamline the data acquisition and data processing tasks.

References

Axelrad, P., C. J. Comp, and P. F. MacDoran (1996), SNR-based multipath error correction for GPS differential phase, *IEEE Trans. Aerosp. Electron. Syst.*, *32*(2), 650–660.

Bilich, A., K. M. Larson, and P. Axelrad (2002), SNR-based multipath corrections to GPS phase measurements, *Eos Trans. AGU*, *83*(47), Fall Meet. Suppl., abstract G22A-06.

Bilich, A., K. M. Larson, and P. Axelrad (2003), Observations of signal-to-noise ratios (SNR) at geodetic GPS site CASA: Implications for phase multipath, paper presented at the Workshop The State of GPS Vertical Positioning Precision: Separation of Earth Processes by Space Geodesy, IAG, Luxembourg, 2–4 Apr.

Bock, Y., R. M. Nikolaidis, P. J. de Jonge, and M. Bevis (2000), Instantaneous geodetic positioning at medium distances with the Global Positioning System, *J. Geophys. Res.*, *105*, 28,223–28,253.

Brunner, F. K., H. Hartinger, and L. Troyer (1999), GPS signal diffraction modeling: The stochastic SIGMA-Δ model, *J. Geodesy*, *73*, 259–267.

Byun, S. H., G. A. Hajj, and L. E. Young (2002), Development and application of GPS signal multipath simulator, *Radio Sci.*, *37*(6), 1098, doi:10.1029/2001RS002549.

Counselman, C. C. (1999), Multipath-rejecting GPS antennas, *Proc. IEEE*, *87*(1), 86–91.

Davis, J. L., T. A. Herring, I. I. Shapiro, A. E. E. Rogers, and G. Elgered (1985), Geodesy by radio interferometry: Effects of atmospheric modeling errors on estimates of baseline length, *Radio Sci.*, *20*, 1593–1607.

Elósegui, P., J. L. Davis, R. T. K. Jaldehag, J. M. Johansson, A. E. Niell, and I. I. Shapiro (1995), Geodesy using the Global Positioning System: The effects of signal scattering on estimates of site position, *J. Geophys. Res.*, *100*, 9921–9934.

Genrich, J. F., and Y. Bock (1992), Rapid resolution of crustal motion at short ranges with Global Positioning System, *J. Geophys. Res.*, *97*, 3261–3269.

Georgiadou, Y., and A. Kleusberg (1988), On carrier signal multipath effects in relative GPS positioning, *Manuscr. Geod.*, *13*, 172–179.

Hurst, K. J., and Y. Bar-Sever (1998), Site specific phase center maps for GPS stations, *Eos Trans. AGU*, *79*(45), Fall Meet. Suppl., abstract G71B-13.

Jaldehag, R. K., J. M. Johansson, B. O. Rönnäng, P. Elósegui, J. L. Davis, I. I. Shapiro, and A. E. Niell (1996), Geodesy using the Swedish permanent GPS network: Effects of signal scattering on estimates of site position, *J. Geophys. Res.*, *101*, 17,841–17,860.

Larson, K., P. Bodin, and J. Gomberg (2003), Using 1 Hz GPS data to measure deformations caused by the Denali fault earthquake, *Science*, *300*, 1421–1424.

Leick, A. (1995), *GPS Satellite Surveying*, 2nd ed., 560 pp., John Wiley, Hoboken, N. J.

Mader, G. L., and J. R. MacKay (1996), Calibration of GPS antennas, in *IGS Workshop; 1996 IGS Analysis Center Workshop*, edited by R. E. Neilan, P. Van Scoy, and J. F. Zumberge, pp. 81–105, IGS Cent. Bur., Jet Propulsion Lab., Pasadena, Calif.

Meertens, C., C. Alber, J. Braun, C. Rocken, B. Stephens, R. Ware, M. Exner, and P. Kolesnikoff (1996), Field and anechoic chamber tests of GPS antennas, in *IGS Workshop; 1996 IGS Analysis Center Workshop*, edited by R. E. Neilan, P. Van Scoy, and J. F. Zumberge, pp. 107–118, IGS Cent. Bur., Jet Propulsion Lab., Pasadena, Calif.

Reichert, A. K. (1999), Correction algorithms for GPS carrier phase multipath utilizing the signal-to-noise ratio and spatial correlation, Ph.D. thesis, Univ. of Colo., Boulder.

Rothacher, M., S. Schaer, L. Mervart, and G. Beutler (1995), Determination of antenna phase center variations using GPS data, in *IGS Workshop; Special Topics and New Directions*, edited by G. Gendt and G. Dick, pp. 205–220, IGS Cent. Bur., Jet Propulsion Lab., Pasadena, Calif.

Scappuzzo, F. S. (1997), Phase multipath estimation for Global Positioning System (GPS) using signal-to-noise-ratio (SNR) data, M.S. thesis, Mass. Inst. of Technol., Cambridge, Mass.

Schmid, R., and M. Rothacher (2003), Estimation of elevation-dependent satellite antenna phase center variations of GPS satellites, *J. Geodesy*, *77*, 440–446.

Schupler, B. R., and T. A. Clark (2001), Characterizing the behavior of geodetic GPS antennas, *GPS World*, *12*(2), 48–55.

Schupler, B. R., R. L. Allshouse, and T. A. Clark (1994), Signal characteristics of GPS user antennas, *J. Inst. Navig.*, *41*, 277–295.

Tranquilla, J. M., J. P. Carr, and H. M. Al-Rizzo (1994), Analysis of a choke ring groundplane for multipath control in Global Positioning System (GPS) applications, *IEEE Trans. Antennas Propagat.*, *42*(7), 905–911.

Wdowinski, S., Y. Bock, J. Zhang, and P. Fang (1997), Southern California permanent GPS geodetic array: Spatial filtering of daily positions for estimating coseismic and postseismic displacements induced by the 1992 Landers earthquake, *J. Geophys. Res.*, *102*, 18,057–18,070.

Weill, R. L. (2002), Multipath mitigation using modernized GPS signals: How good can it get?, in *ION GPS 2002: 15th International Technical Meeting of the Satellite*

Division of the Institute of Navigation, pp. 493–505, Inst. of Navig., Fairfax, Va.

Wübbena, G., M. Schmitz, F. Menge, V. Boder, and G. Seeber (2000), Automated absolute field calibration of GPS antennas in real-time, in *ION GPS 2000: 13th International Technical Meeting of the Satellite Division of the Institute of Navigation*, pp. 2512–2522, Inst. of Navig., Fairfax, Va.

————————

V. A. Andreatta, C. E. Meertens, and J. E. Normandeau, UNAVCO, Inc., 6350 Nautilus Drive, Boulder, CO 80301, USA. (andreatta@unavco.org; meertens@unavco.org; normandeau@unavco.org)

B. E. Corey and A. E. Niell, MIT Haystack Observatory, Westford, MA 01886, USA. (bcorey@haystack.mit.edu; aniell@haystack.mit.edu)

J. L. Davis and P. Elósegui, Harvard-Smithsonian Center for Astrophysics, 60 Garden St., MS 42, Cambridge, MA 02138, USA. (jdavis@cfa.harvard.edu; pelosegui@cfa.harvard.edu)

P. O. J. Jarlemark, SP Swedish National Testing and Research Institute, Box 857, Borås SE-501 15, Sweden. (per.jarlemark@sp.se)

K.-D. Park, College of Forest Science, Kookmin University, 861-1 Jungnung-dong Sungbuk-gu, Seoul 136-702, Korea. (kdpark@kookmin.ac.kr)